Chapter 6

Metal Doped TiO_2-ZrO_2 Composites

6.1 Metal Doped TiO_2-ZrO_2 Composite

Doping can affect the electrical, structural and optical properties of the material **[1-4]**. The phase transformation of TiO_2 depends on impurities, type of dopant and amount of dopant. The bandgap of the material can be varied by adding impurities. It has been reported that transition and rare earth metal ions shift the absorption edge towards visible region **[5-8]**. For Dye Sensitized Solar Cell application material should have low recombination rate of electron-hole pairs and this can be eliminated by transition metal and rare earth ions doping.

6.2 Synthesis of Samples

A set of metal (Al, Cu, Mg, Zn, Ce, La, Eu, Fe, Ni, Mn, Er, Cd, Yb and Pb) doped TiO_2-ZrO_2 composites were prepared by the hydrothermal method. TiO_2-ZrO_2 composites were doped with 2 mol% of metal ions. Titanium isopropoxide, Zirconium propoxide and isopropanol were used as starting chemicals. All chemicals were analytical grade and used as received. The synthesis was carried out as follows: Ti isopropoxide and Zr propoxide were diluted in isopropanol to obtain mixtures in a 7:3 and $TiO_{2:}$ ZrO_2 molar ratio. Dilute HNO_3 was added drop wise to the alkoxide solution kept under vigorous stirring in an ice bath. 2 mol% Solution of metal nitrate was added to above solution. After alkoxide hydrolysis the alcogel was obtained. The alcogel was transferred to a stainless steel autoclave. The temperature was raised to 240 °C and the sample was maintained under autogenic pressure for 24 h. Then, the sample was oven-dried at 100 °C (2 h) and finally calcined at 450 °C for 4 hours under static air atmosphere. Metal doped mixed oxides in solid form were obtained.

6.3 Characterization of Samples

The structural properties and composition of prepared samples were analyzed by X-ray diffraction. The optical properties of the samples were investigated by UV-Visible spectroscopy.

6.3.1 X-Ray Diffraction Analysis

The XRD patterns were recorded on Bruker D8 Advance X-ray diffractometer in 2θ range of 20^0 to 90^0 at room temperature. The XRD patterns of prepared samples are given in figure 1 to 14 their structural parameters are given in Table 1 to 14. The presence of both the oxides was confirmed form the comparison of d values with JCPDS data base (Anatase TiO_2-21-1272, Rutile TiO_2-21-1276, Monoclinic ZrO_2-83-0944, and Tetragonal ZrO_2-79-1770). The d values match very closely with JCPDS data.

All the samples show distinct peaks with good intensity and broadening. The pattern indicates high degree of crystallinity and formation of material in nanocrystalline size. Infect the crystallinity of the doped samples have been found to be better than the undoped TiO_2-ZrO_2 samples. Hence the dopant appeared to be playing significant role in enhancing the crystallinity of the samples. The average crystallite size of the samples lies between 6.02 nm to 22.39 nm

The Anatase peak of TiO_2 (101) is the dominant feature in all the samples except the one doped with iron. Apart from the (101) peak the other common Anatase peaks are for the planes (004), (200) and (204) were observed. Rutile content is significantly low.

Amongst the ZrO_2 peaks the ones for (101) of Tetragonal phase are the most common. Apart from that the other common Monoclinic peaks for the planes (122) and (041) were observed.

The most intense Anatase (101) peaks have been observed for the samples doped with lead, cadmium and ytterbium. The samples doped with Al, Cu, Mg, Zn and Eu show moderate intensities while the ones doped with Ce, La, Fe, Ni, Mn and Er show low intensities which is shown in figure. A clear understanding of this shown in figure 15.

The samples doped with iron gives a different pattern with several prominent peaks of Rutile phase. This sample shows the lowest Anatase content and highest crystallite size. The Fe ion could not inhibit the crystallization and hence Anatase phase converted to Rutile. It has been reported that iron dopant enlarges the lattice parameter which could be the reason for larger crystallite size **[m]**.

The metal doping appears to be stabilizing the Anatase phase and increases the Anatase mass fraction which results into lower crystallite size **[l]**. The lowest Anatase mass fraction is observed for Fe doped TiO_2-ZrO_2 composite.

The samples doped with Fe, Cd, Yb and Pb show small amount of strain. Fe doped TiO_2-ZrO_2 composite is highly crystalline material this could be the reason for lower strain **[n]**. The presence of pure single Anatase phase of TiO_2 in Cd, Yb, and Pb doped samples could be responsible for its lower strain values, as mixed phases can produce strain at grain boundaries. The crystallinity index is given in Table 15 samples doped with Cd, Yb and Pb show highest values.

The lattice parameters vary in very short range which shows the formation of uniform crystal structure.

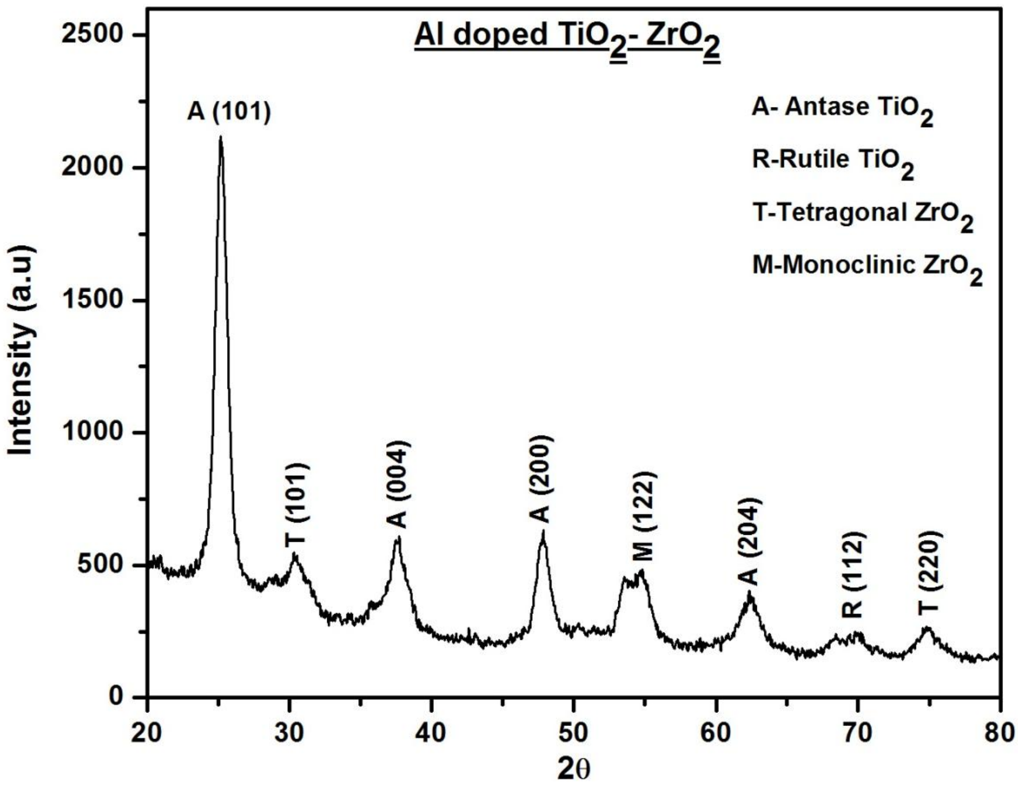

Figure 1: XRD pattern of sample Al doped TiO_2-ZrO_2 composite

Table 1: Structural parameters of Al doped TiO_2-ZrO_2 composite

Experimental d values	JCPDS d values	Crystallite size (nm)	Strain (%)	Anatase content (%)
3.53564	3.5200	8.85	0.078	
2.94484	2.9529	--	--	
2.38145	2.3780	5.49	0.085	
1.89911	1.8920	8.06	0.046	**86.58**
1.67281	1.6752	4.09	0.080	
1.48822	1.4808	5.36	0.054	
1.34601	1.3465	3.62	0.073	
1.27117	1.2639	6.12	0.040	

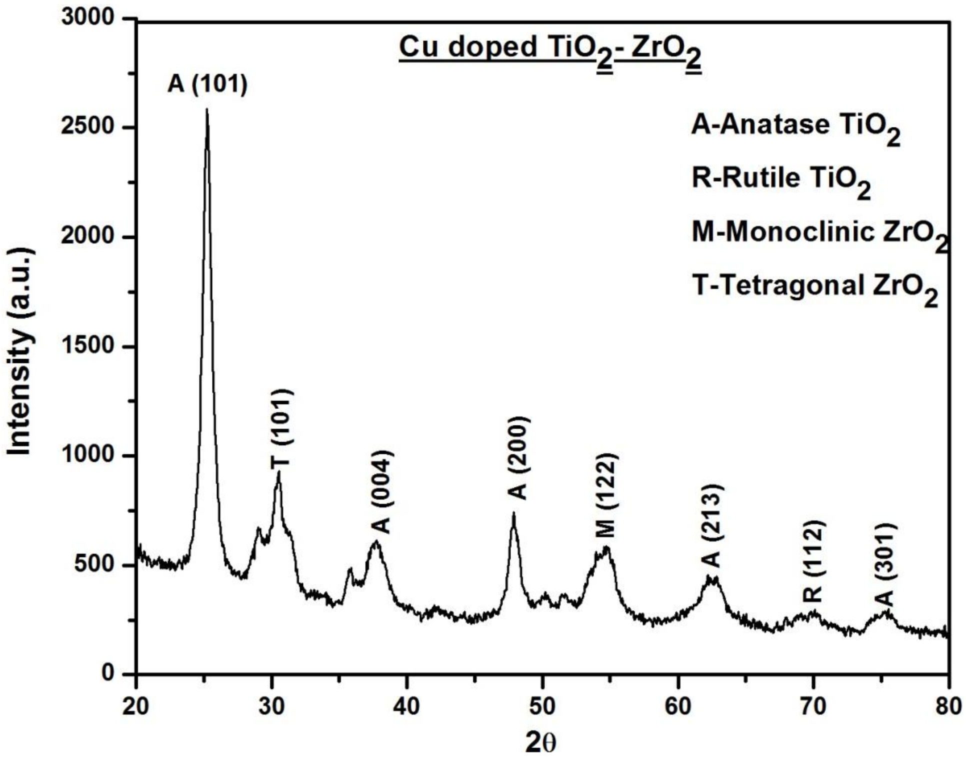

Figure 2: XRD pattern of sample Cu doped TiO_2-ZrO_2 composite

Table 2: Structural parameters of Cu doped TiO_2-ZrO_2 composite

Experimental d values	JCPDS d values	Crystallite size (nm)	Strain (%)	Anatase content (%)
3.5275	3.5200	10.30	0.067	
2.9255	2.9529	7.96	0.072	
2.3743	2.3780	5.57	0.083	
1.8980	1.8920	9.80	0.038	**86.99**
1.6752	1.6752	4.52	0.072	
1.4907	1.4930	4.83	0.060	
1.3411	1.3465	3.98	0.066	
1.2572	1.2509	4.71	0.052	

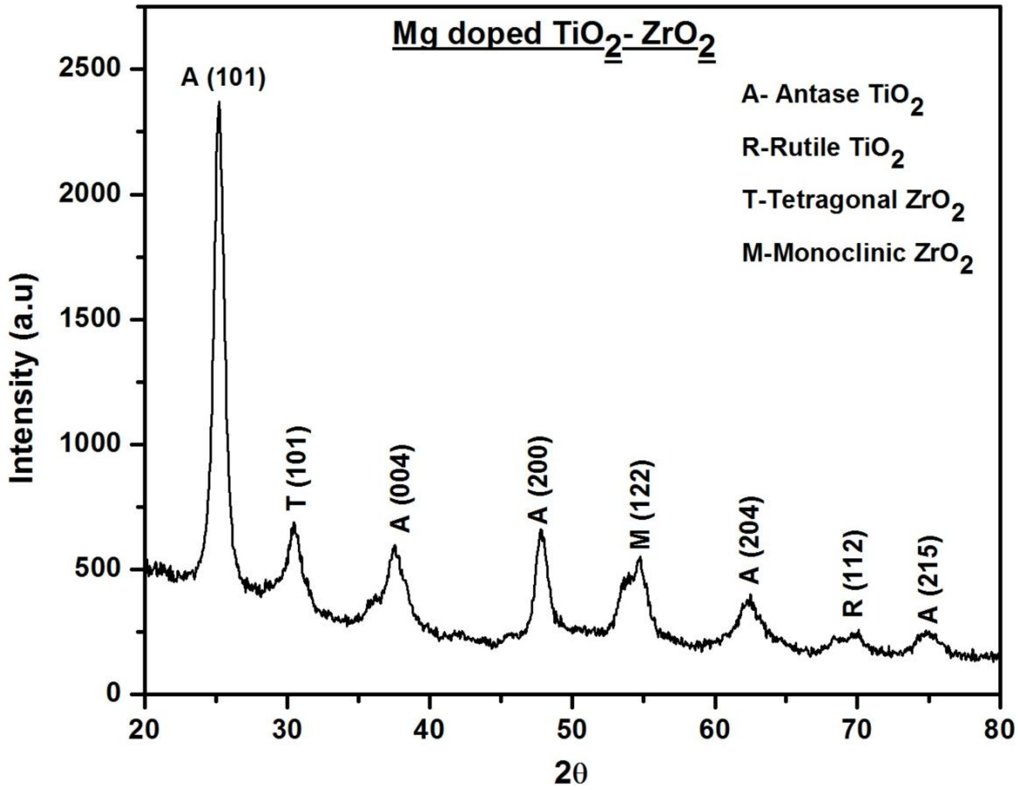

Figure 3: XRD pattern of sample Mg doped TiO_2-ZrO_2 composite

Table 3: Structural parameters of Mg doped TiO_2-ZrO_2 composite

Experimental d values	JCPDS d values	Crystallite size (nm)	Strain (%)	Anatase content (%)
3.5275	3.5200	8.95	0.077	
2.9310	2.9529	8.38	0.068	
2.3922	2.3780	6.22	0.075	
1.9002	1.8920	8.73	0.042	**87.28**
1.6744	1.6752	4.88	0.067	
1.4838	1.4808	5.18	0.056	
1.3415	1.3465	6.45	0.040	
1.2639	1.2649	6.66	0.037	

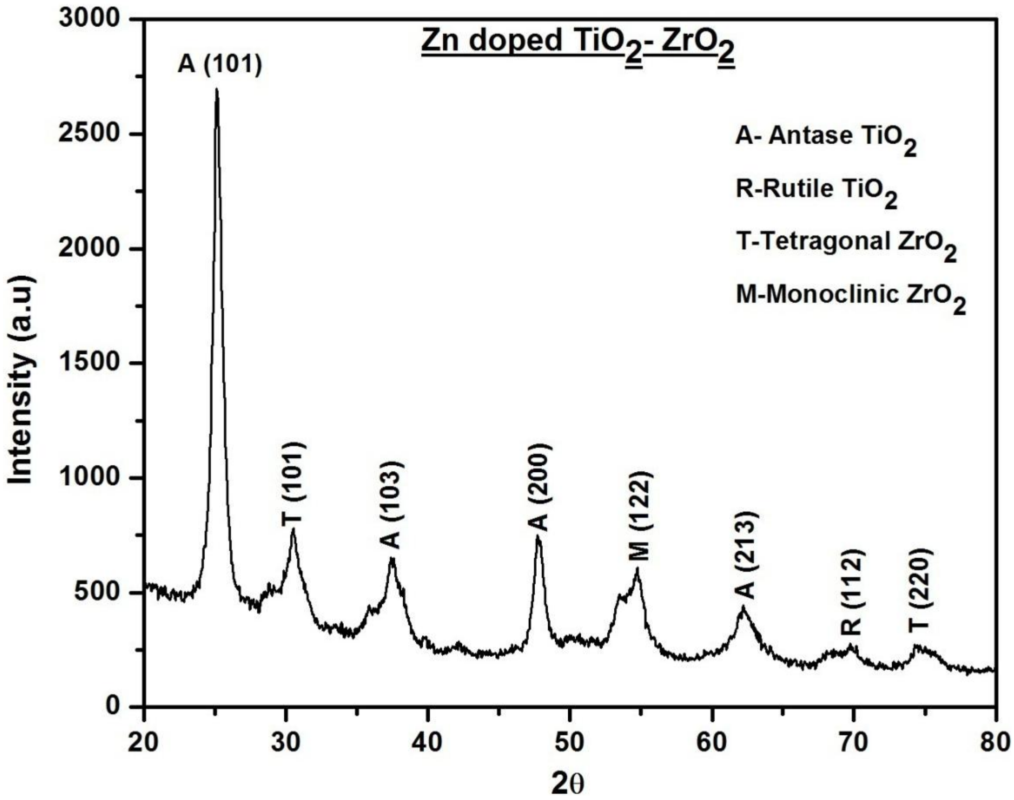

Figure 4: XRD pattern of sample Zn doped TiO_2-ZrO_2 composite

Table 4: Structural parameters of Zn doped TiO_2-ZrO_2 composite

Experimental d values	JCPDS d values	Crystallite size (nm)	Strain (%)	Anatase content (%)
3.5397	3.5200	10.45	0.066	
2.9282	2.9529	6.99	0.082	
2.4012	2.4310	5.81	0.081	
1.9035	1.8920	10.25	0.036	**88.02**
1.6744	1.6752	4.45	0.074	
1.4901	1.4930	6.02	0.048	
1.3465	1.3465	4.03	0.065	
1.2707	1.2705	5.02	0.049	

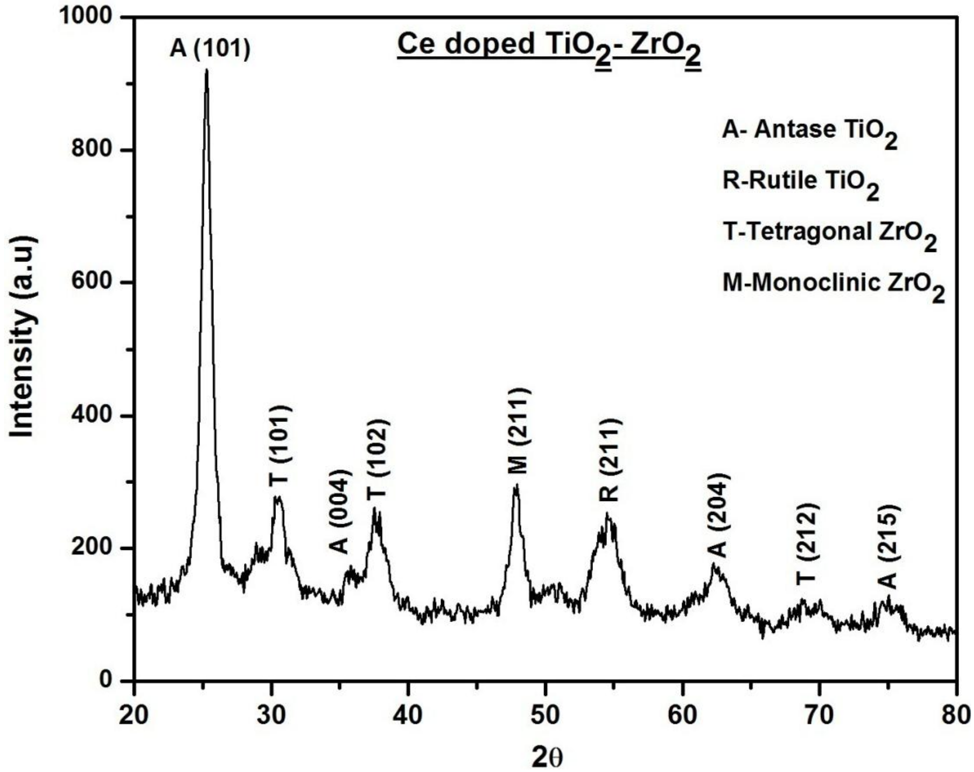

Figure 5: XRD pattern of sample Ce doped TiO_2-ZrO_2 composite

Table 5: Structural parameters of Ce doped TiO_2-ZrO_2 composite

Experimental d values	JCPDS d values	Crystallite size (nm)	Strain (%)	Anatase content (%)
3.5208	3.5200	9.18	0.075	
2.9224	2.9529	8.45	0.068	
2.3932	2.3780	5.50	0.085	
2.1256	2.1015	--	--	**73.73**
1.9019	1.9893	8.61	0.043	
1.6817	1.6874	4.19	0.078	
1.4879	1.4808	4.48	0.065	
1.3687	1.3656	3.28	0.081	
1.2648	1.2649	4.45	0.055	

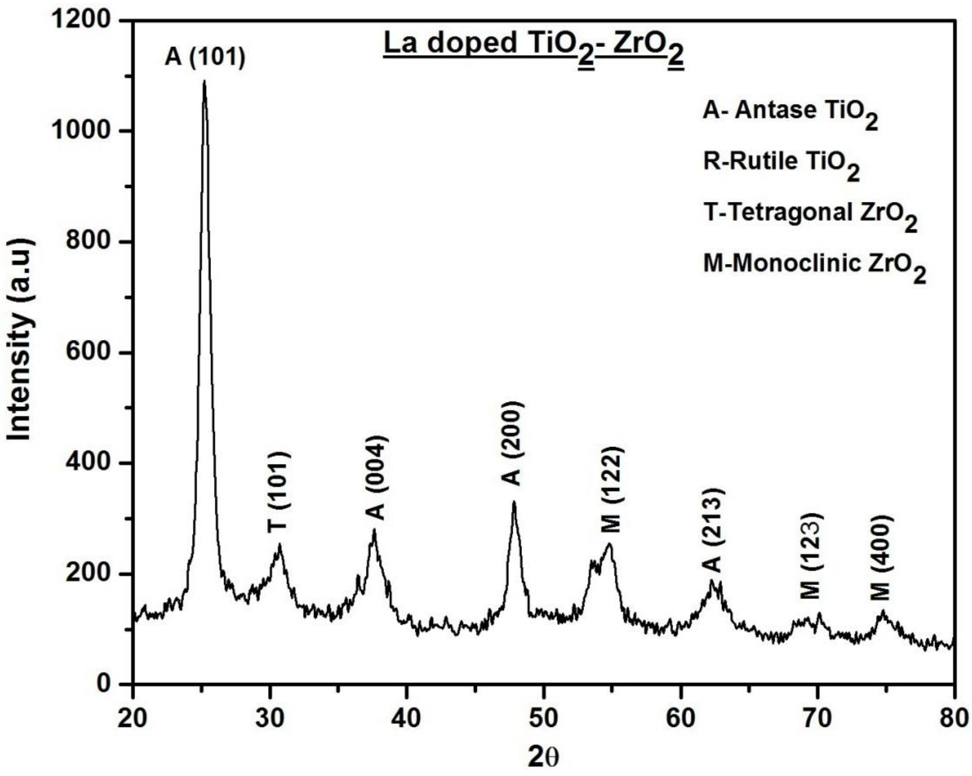

Figure 6: XRD pattern of sample La doped TiO_2-ZrO_2 composite

Table 6: Structural parameters of La doped TiO_2-ZrO_2 composite

Experimental d values	JCPDS d values	Crystallite size (nm)	Strain (%)	Anatase content (%)
3.53459	3.5200	9.94	0.076	
2.90856	2.9529	7.57	0.010	
2.38709	2.378	6.08	0.054	
1.90007		8.44	0.041	
1.89821	1.8920	--	--	
1.67467	1.6752	4.61	--	**86.26**
1.48898	1.4948	3.99	0.010	
1.48791	1.4808	--	0.074	
1.34141	1.3465	3.75	0.009	
1.33975	1.3381	--	--	
1.26773	1.2649	4.68	0.031	

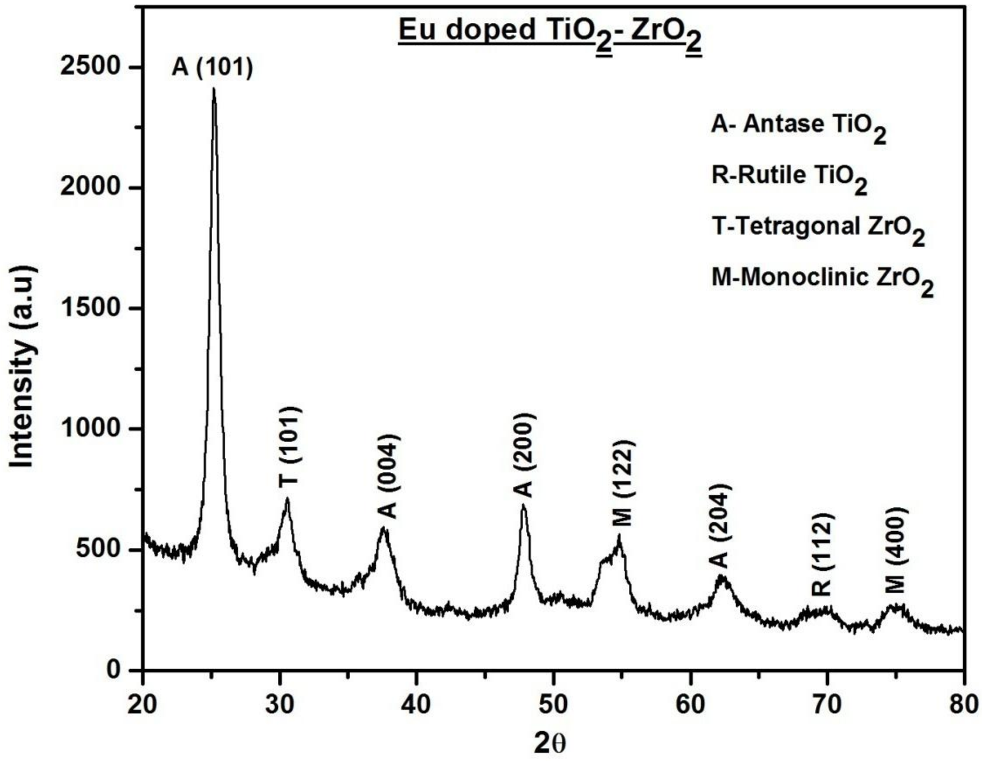

Figure 7: XRD pattern of sample Eu doped TiO_2-ZrO_2 composite

Table 7: Structural parameters of Eu doped TiO_2-ZrO_2 composite

Experimental d values	JCPDS d values	Crystallite size (nm)	Strain (%)	Anatase content (%)
3.5235	3.5200	10.10	0.068	
2.9310	2.9529	8.18	0.070	
2.3814	2.378	4.37	0.107	
1.8980	1.8920	9.36	0.039	**86.41**
1.6695	1.6665	4.37	0.075	
1.4875	1.4808	5.68	0.051	
1.3440	1.3465	4.32	0.061	
1.2681	1.269	5.32	0.046	

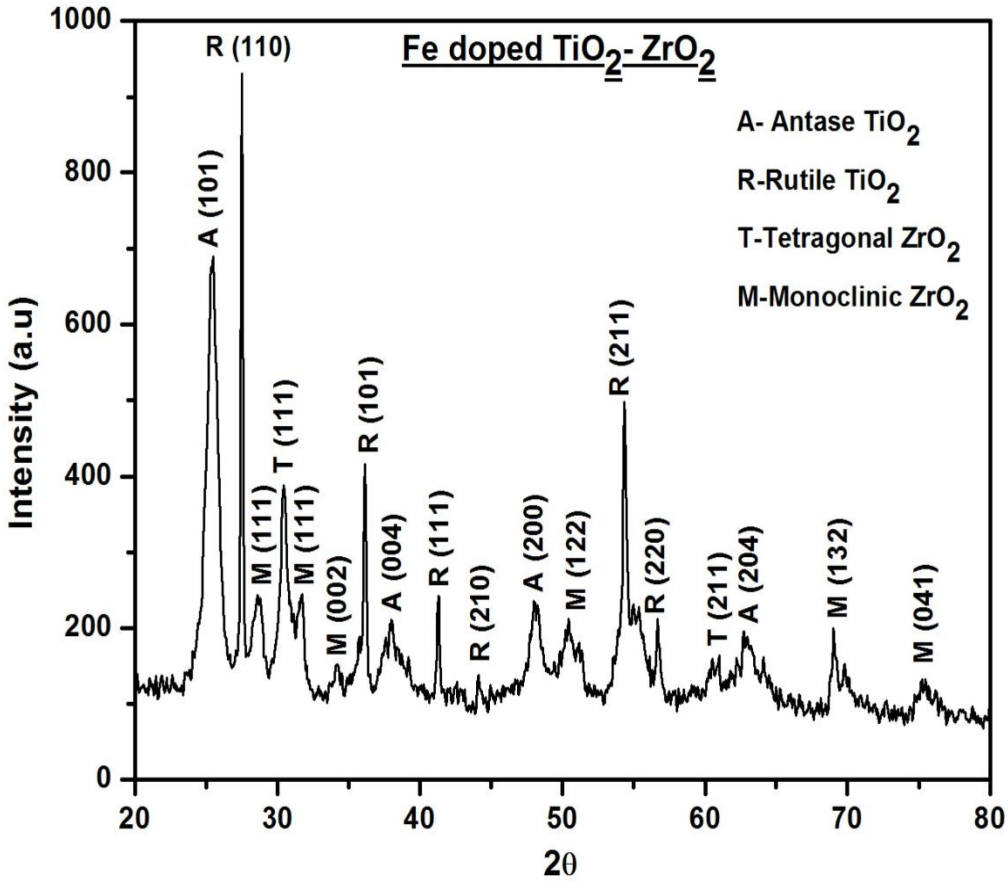

Figure 8: XRD pattern of sample Fe doped TiO_2-ZrO_2 composite

Table 8: Structural parameters of Fe doped TiO_2-ZrO_2 composite

Experimental d values	JCPDS d values	Crystallite size (nm)	Strain (%)	Anatase content (%)
3.4937	3.5200	8.97	0.076	
3.2384	3.2470	58.24	0.010	
3.1166	3.1598	11.25	0.054	
2.9365	2.9529	13.82	0.041	
2.8192	2.8375	--	--	
2.6228	2.6213	--	--	
2.4824	2.4870	44.80	6.6×10^{-4}	
2.3629	2.3780	6.21	0.004	
2.1845	2.1880	46.87	5.5×10^{-4}	
2.0523	2.0540	--	--	
1.8816	1.8920	11.70	0.001	**35.70**
1.8082	1.8012	8.81	0.002	
1.7835	1.7803	--	--	
1.6860	1.6874	29.38	0.011	
1.6230	1.6237	31.47	0.010	
1.5276	1.5349	--	--	
1.4804	1.4808	5.15	0.056	
1.3583	1.3592	17.31	0.015	
1.3464	1.3465	54.95	0.004	
1.2997	1.2953	--	--	
1.2619	1.2617	6.30	0.039	
1.1703	1.1703	2.78	0.082	

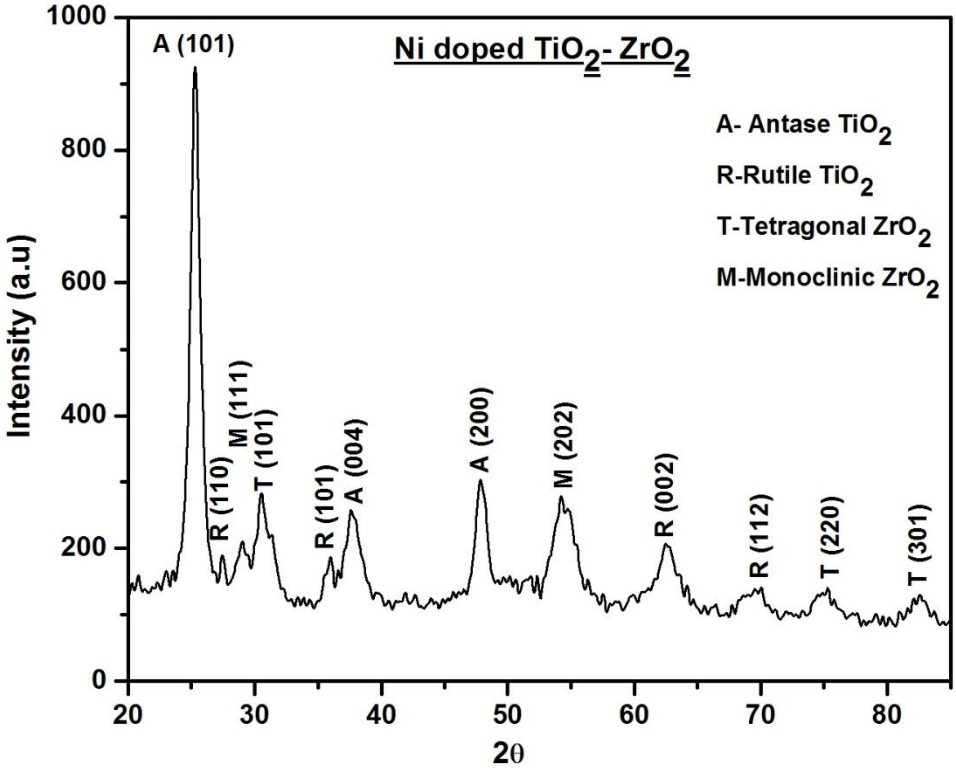

Figure 9: XRD pattern of sample Ni doped TiO_2-ZrO_2 composite

Table 9: Structural parameters of Ni doped TiO_2-ZrO_2 composite

Experimental d values	JCPDS d values	Crystallite size (nm)	Strain (%)	Anatase content (%)
3.5208	3.5200	9.71	0.071	
3.2499	3.2470	28.35	--	
3.0798	3.1598	5.68	0.106	
2.9365	2.9529	8.73	0.066	
2.4891	2.4870	--	--	
2.3932	2.3780	--	--	**79.03**
1.8982	1.8920	8.45	0.044	
1.6903	1.6930	4.51	0.073	
1.4794	1.4797	4.70	0.061	
1.3422	1.3465	4.58	0.057	
1.2713	1.2705	4.70	0.053	
1.1680	1.1670	5.69	0.040	

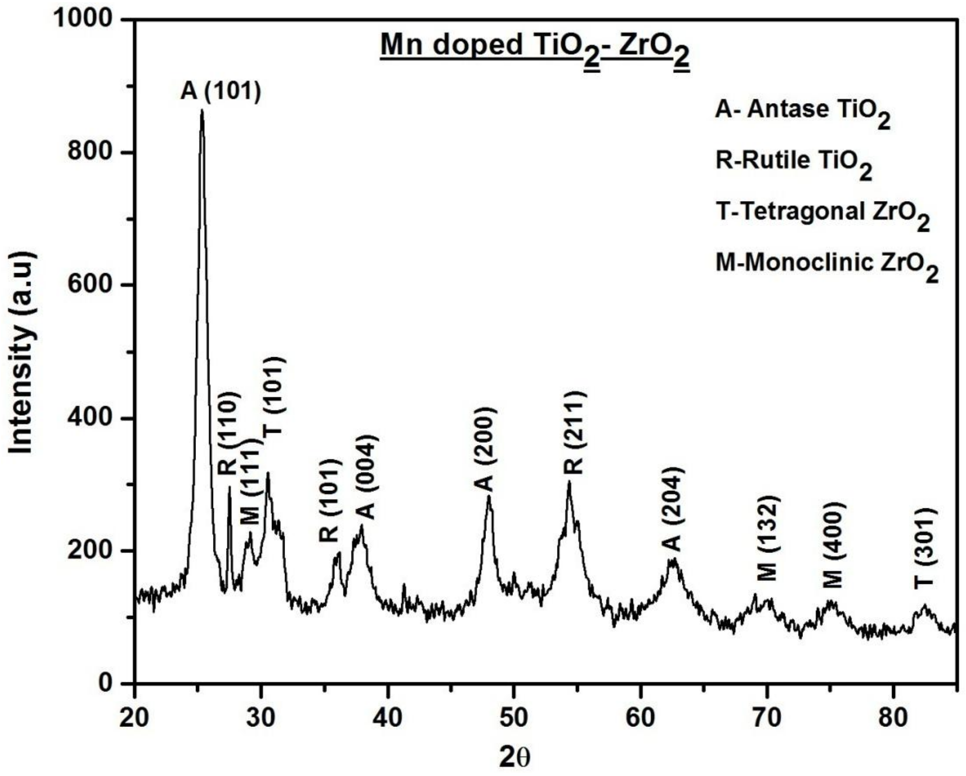

Figure 10: XRD pattern of sample Mn doped TiO_2-ZrO_2 composite

Table 10: Structural parameters of Mn doped TiO_2-ZrO_2 composite

Experimental d values	JCPDS d values	Crystallite size (nm)	Strain (%)	Anatase content (%)
3.5140	3.5200	9.98	0.069	
3.2384	3.2470	47.79	0.013	
3.0541	3.1598	8.87	0.067	
2.9224	2.9529	8.08	0.071	
2.4791	2.4870	10.13	0.048	
2.3689	2.3780	6.88	0.067	**68.89**
1.8908	1.8920	9.32	0.039	
1.6860	1.6874	5.34	0.062	
1.4804	1.4808	3.85	0.075	
1.3583	1.3592	3.14	0.084	
1.2677	1.2690	4.71	0.052	
1.1680	1.1670	6.34	0.036	

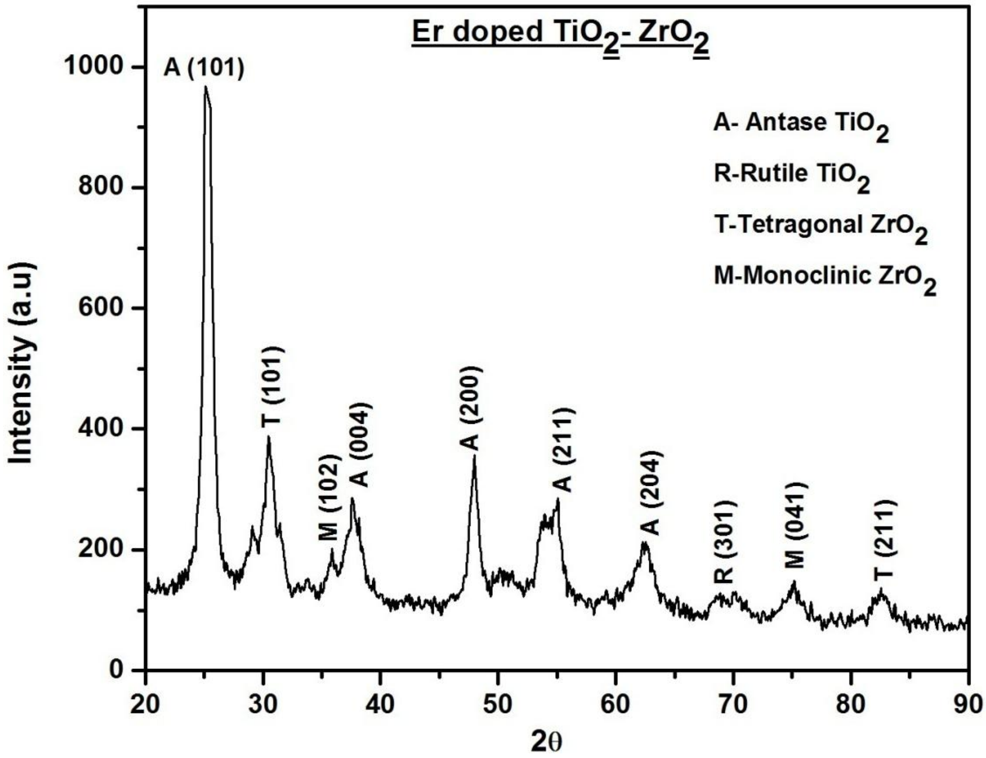

Figure 11: XRD pattern of sample Er doped TiO_2-ZrO_2 composite

Table 11: Structural parameters of Er doped TiO_2-ZrO_2 composite

Experimental d values	JCPDS d values	Crystallite size (nm)	Strain (%)	Anatase content (%)
3.5415	3.5200	9.11	0.076	
3.0643	3.1598	--	--	
2.9318	2.9507	8.60	0.067	
2.4991	2.4976	--	--	
2.3932	2.3780	5.45	0.086	
1.8926	1.8920	10.66	0.034	**84.6**7
1.6662	1.6665	4.51	0.072	
1.4836	1.4808	5.33	0.054	
1.3574	1.3598	3.08	0.086	
1.2627	1.2617	7.00	0.035	
1.1537	1.1531	3.80	0.059	

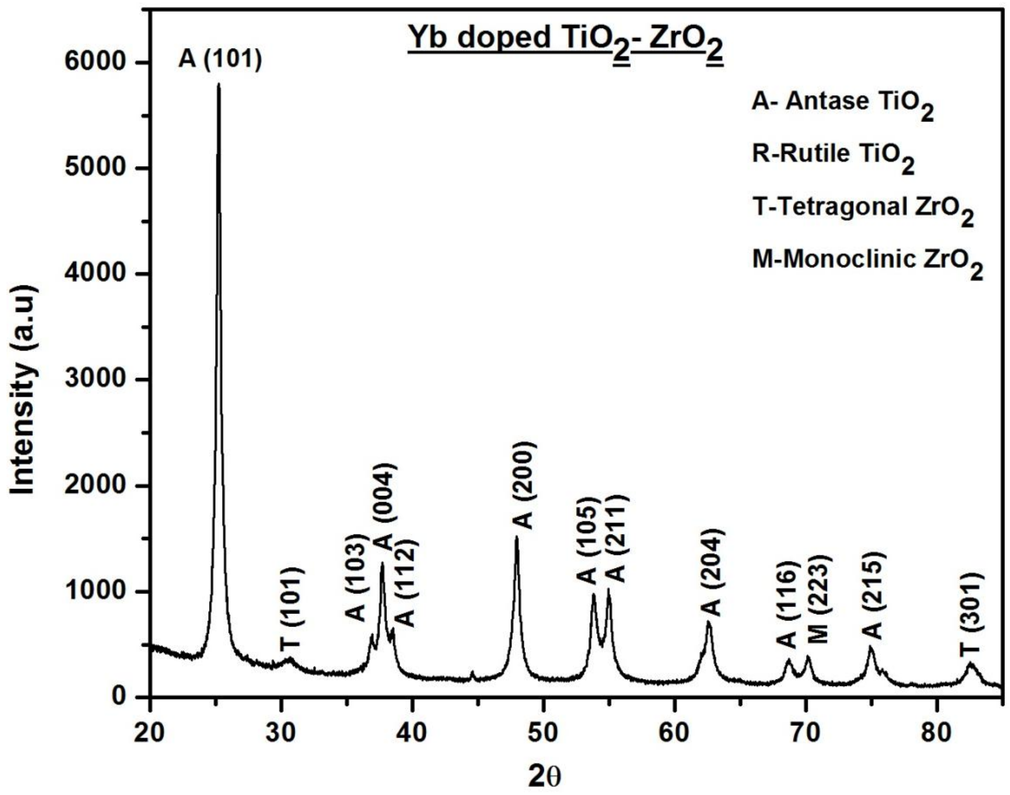

Figure 12: XRD pattern of sample Yb doped TiO_2-ZrO_2 composite

Table 12: Structural parameters of Yb doped TiO_2-ZrO_2 composite

Experimental d values	JCPDS d values	Crystallite size (nm)	Strain (%)	Anatase content (%)
3.52669	3.5200	20.93	0.033	
2.90381	2.9529	--	--	
2.43227	2.4310	16.10	0.029	
2.33408	2.3320	18.50	0.020	
1.89405	1.8920	12.77	0.026	
1.70145	1.6990	15.18	0.021	**100**
1.66869	1.6665	10.36	0.028	
1.48291	1.4808	11.14	0.024	
1.36383	1.3641	12.34	0.021	
1.33896	1.3381	12.01	0.020	
1.26587	1.2649	8.99	0.025	
1.16743	1.1670	20.93	0.033	

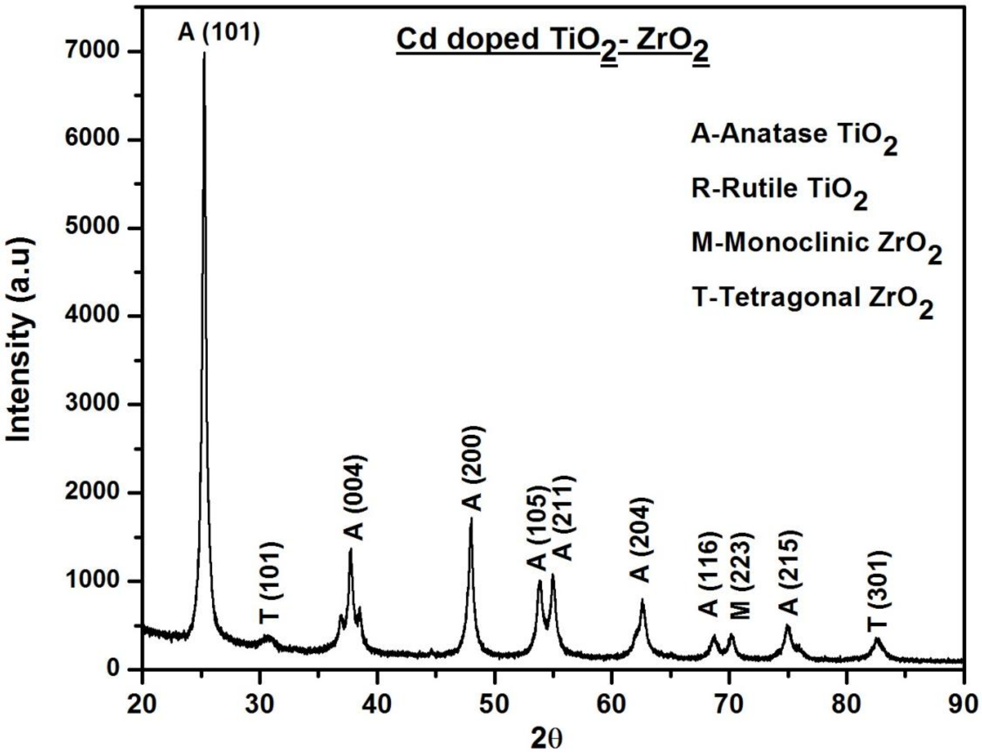

Figure 13: XRD pattern of sample Cd doped TiO_2-ZrO_2 composite

Table 13: Structural parameters of Cd doped TiO_2-ZrO_2 composite

Experimental d values	JCPDS d values	Crystallite size (nm)	Strain (%)	Anatase content (%)
3.5221	3.5200	22.63	0.030	
2.9412	2.9529	--	--	
2.3803	2.3780	15.89	0.029	
1.8928	1.8920	16.16	0.023	
1.7007	1.6990	9.69	0.034	
1.6687	1.6650	13.56	0.024	100
1.4824	1.4808	9.82	0.029	
1.3637	1.3641	9.37	0.028	
1.3392	1.3381	10.88	0.024	
1.2656	1.2649	10.42	0.023	
1.1674	1.1670	7.08	0.032	

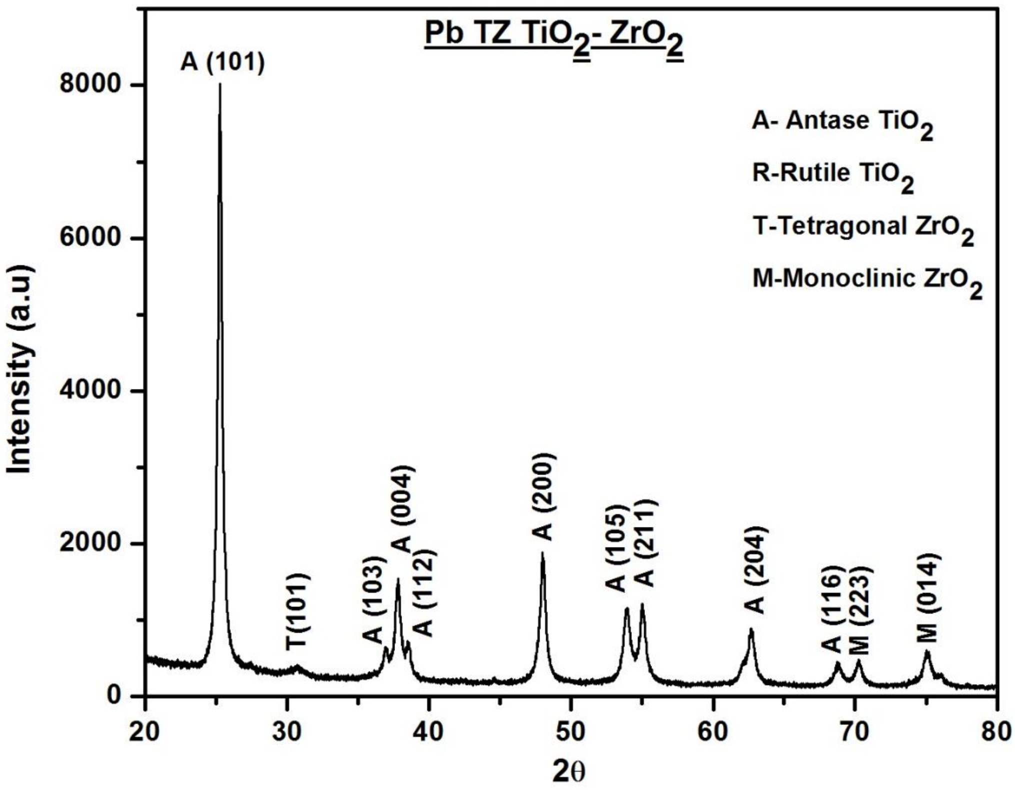

Figure 14: XRD pattern of sample Pb doped TiO_2-ZrO_2 composite

Table 14: Structural parameters of Pb doped TiO_2-ZrO_2 composite

Experimental d values	JCPDS d values	Crystallite size (nm)	Strain (%)	Anatase content (%)
3.51831	3.5200	25.70	0.026	
2.90897	2.9529	--	--	
2.37612	2.3780	18.50	0.025	
2.33637	2.3320	--	--	
1.89271	1.8920	18.50	0.020	
1.6982	1.6999	15.15	0.022	**100**
1.66768	1.6665	16.98	0.019	
1.4809	1.4808	14.17	0.020	
1.36481	1.3641	13.40	0.020	
1.33823	1.3381	15.35	0.017	
1.26259	1.2699	13.07	0.019	

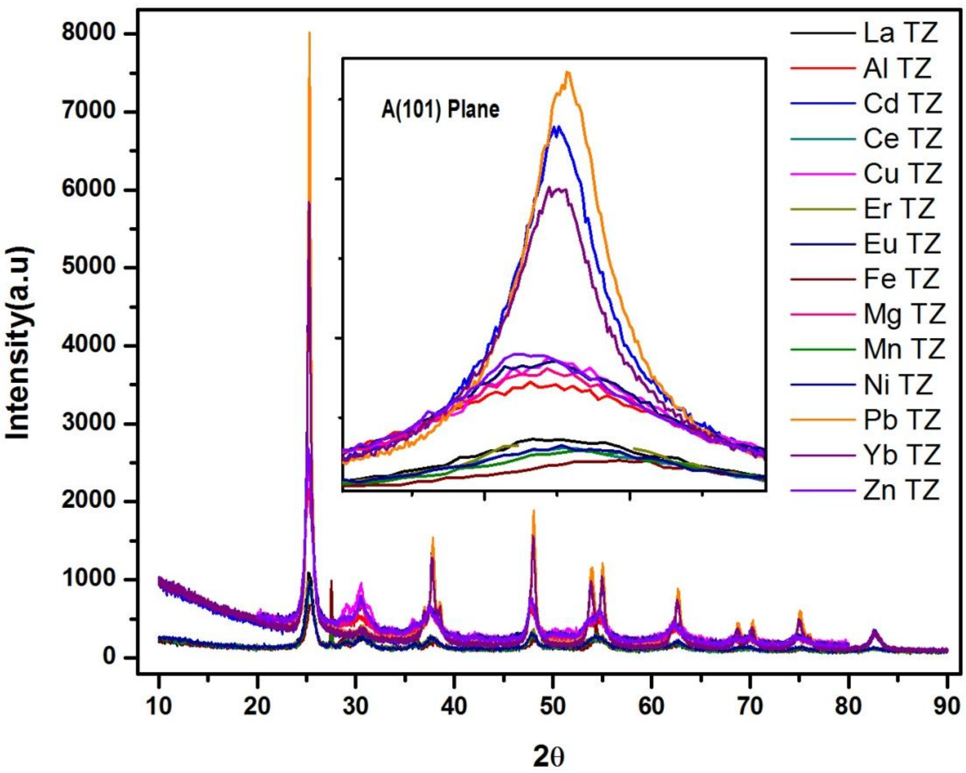

Figure 15: Overlay of XRD patterns of metal doped TiO_2-ZrO_2 composite

Table 15: Structural parameters of metal doped TiO_2-ZrO_2 composite

Sample	Crystallite Size	Anatase Content	Strain	Crystallinity Index	Lattice Parameters Anatase Phase	
					a	c
Al doped TZ	8.16 nm	86.58%	0.046	79.08%	3.80	9.52
Cu doped TZ	6.22 nm	86.99%	0.064	81.40%	3.79	9.50
Mg doped TZ	6.92 nm	87.28%	0.058	80.50%	3.80	9.57
Zn doped TZ	6.31nm	88.03%	0.063	82.60%	3.81	9.61
Ce doped TZ	6.02 nm	73.73%	0.069	86.20%	3.78	9.57
La doped TZ	6.13 nm	100%	0.066	89.14%	3.79	9.55
Eu doped TZ	6.47 nm	86.41%	0.065	80.96%	3.79	9.52
Fe doped TZ	22.39 nm	35.69%	0.026	84.74%	3.76	9.61
Ni doped TZ	6.31 nm	79.02%	0.064	85.83%	3.79	9.57
Mn doped TZ	6.97 nm	68.89%	0.057	85.72%	3.78	9.47
Er doped TZ	6.39 nm	84.66%	0.064	86.41%	3.78	9.57
Cd doped TZ	12.55 nm	100%	0.028	93.19%	3.78	9.53
Yb doped TZ	13.83 nm	100%	0.025	94.29%	3.79	9.53
Pb doped TZ	16.76 nm	100%	0.021	95.21%	3.78	9.50

6.3.2 UV-Visible Spectroscopy

The absorption spectra of the samples were recorded on Thermo Fisher Scientific make Evolution 600 UV-Visible Spectrophotometer in the wavelength range of 200-900 nm. The optical bandgap was calculated by Tauc’s plot. The absorption spectra and related Tauc’s plot are shown in figure 16 to figure 29.

The different optical parameters calculated from UV-Visible absorption spectra are given in Table 16. The following observations can be made from the results.

The peak absorption wavelengths vary in a long range between 249 nm to 365 nm. This is obvious since the incorporation of metal ions even in a single host material can have varied effects on the electrical energy levels of the dopant ion. The ions belong to the transition, alkaline earth metal and rare earth metal groups. Hence there can be a lot of variation.

The optical bandgap is calculated from the Tauc’s plot. The plot is dependent on the absorption edge which in this case varies heavily as can be seen from the absorption plots, which is the reason why the optical bandgap varies from 2.00 eV to 3.34 eV.

Figure 30 shows the variation of absorption coefficient with wavelength. It indicates that there is absorption in all the samples in the visible region as well as in the UV region to some extent. In general the absorption in samples remains on the higher side up to roughly 500 nm and then becomes almost constant.

Samples with Mg, Ni and Cd show very high absorption in UV but comparatively much lower in visible range. Samples doped with La, Eu and Cu do not show much variation in the absorption in UV and visible region. Rest of the samples show moderately high absorption in UV region followed by a flat character in the visible region like other samples.

The variation of extinction coefficient with wavelength is shown in figure 31. Samples doped with Al, Cu, Zn, Eu, Fe and La have high extinction coefficient throughout the visible region and near IR. This indicates higher scattering of light in these samples.

The refractive index of the samples varies with the dopant in the range 2.32 to 2.69. Sample doped with Ni and La shows lowest and highest refractive index respectively.

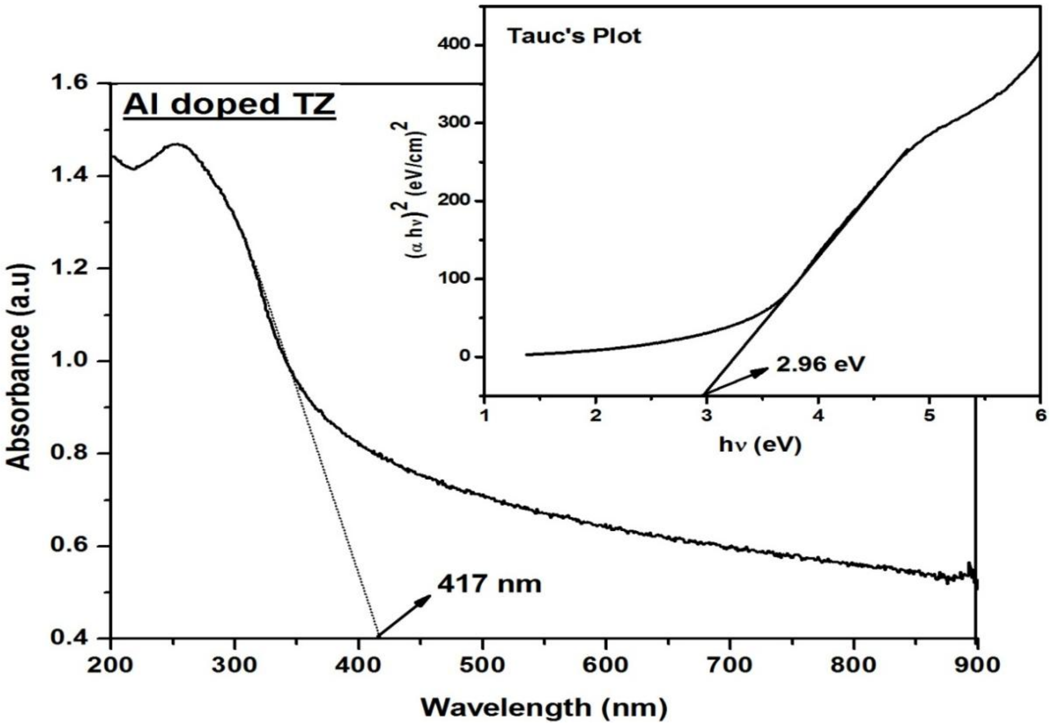

Figure 16: Absorption spectrum and Tauc's plot for Al doped TiO_2-ZrO_2 composite

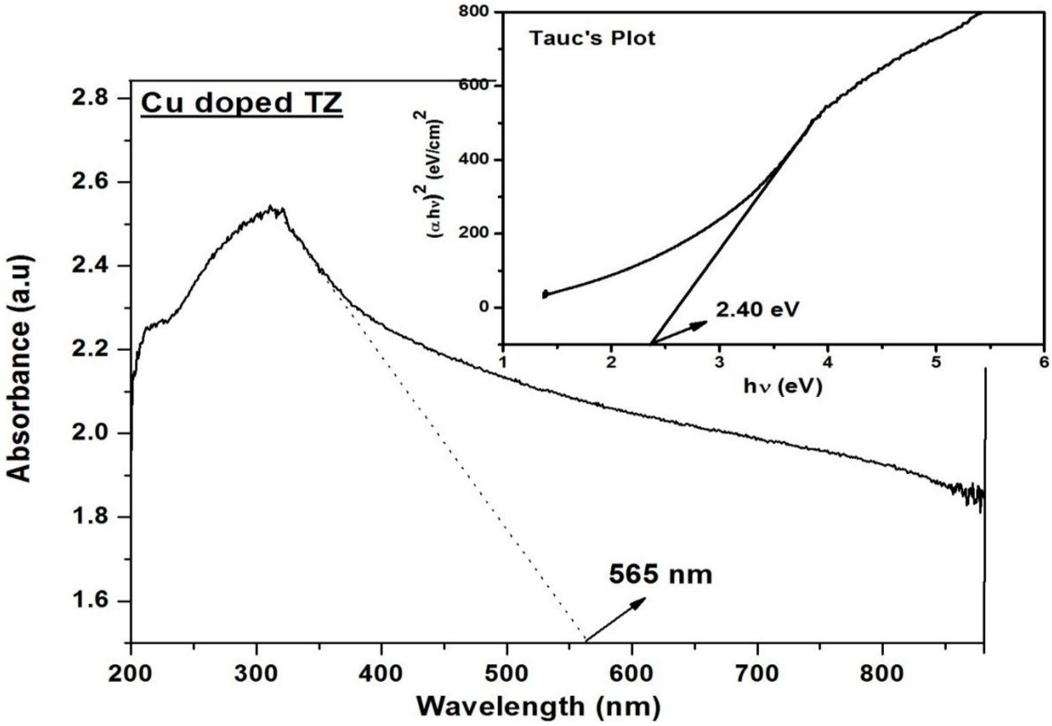

Figure 17: Absorption spectrum and Tauc's plot for Cu doped TiO_2-ZrO_2 composite

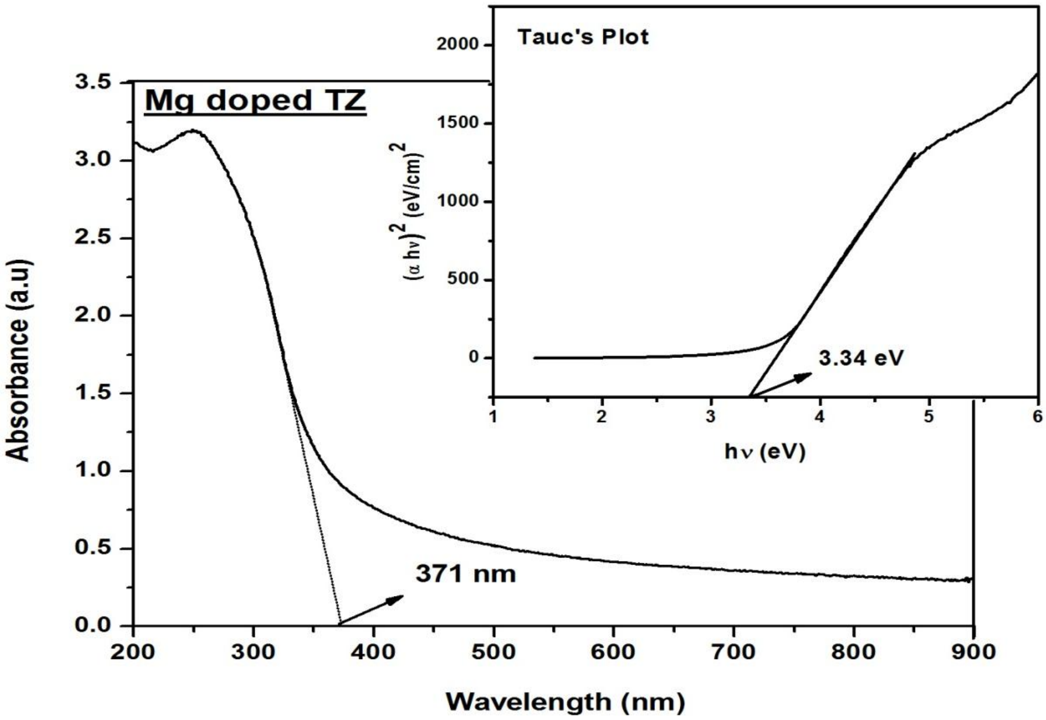

Figure 18: Absorption spectrum and Tauc's plot for Mg doped TiO_2-ZrO_2 composite

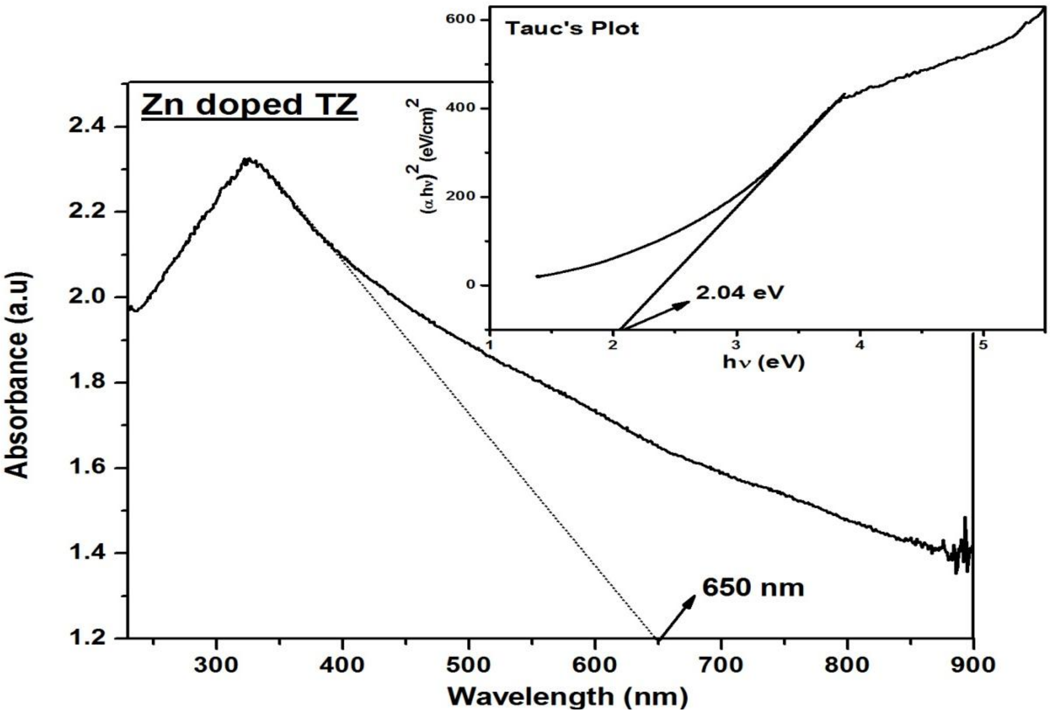

Figure 19: Absorption spectrum and Tauc's plot for Zn doped TiO_2-ZrO_2 composite

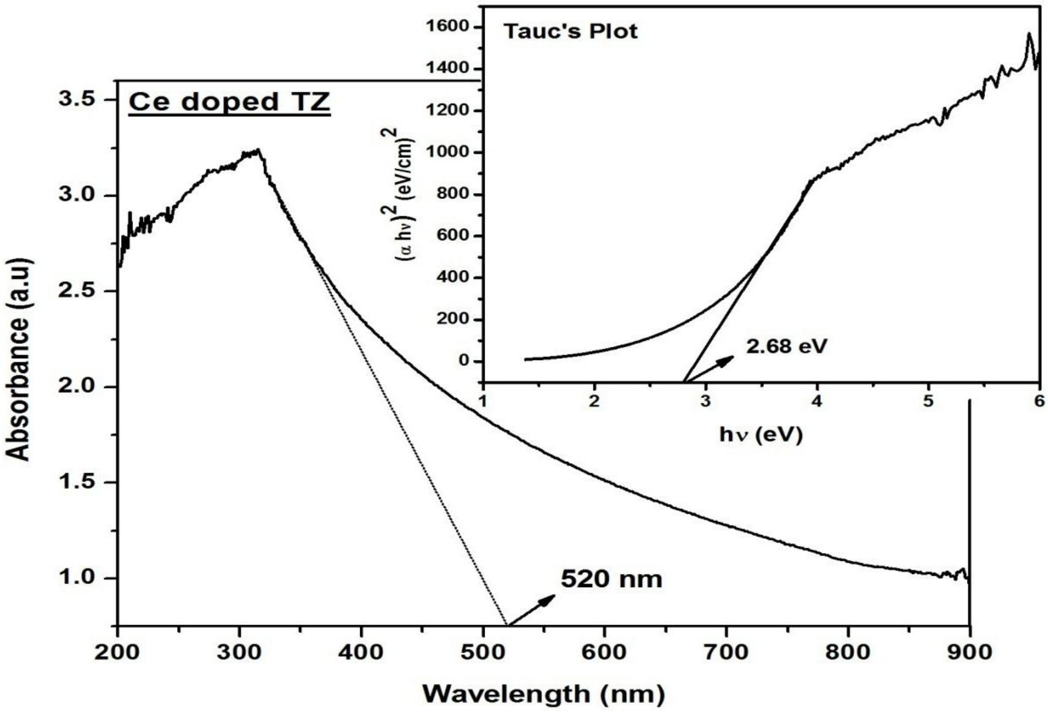

Figure 20: Absorption spectrum and Tauc's plot for Ce doped TiO_2-ZrO_2 composite

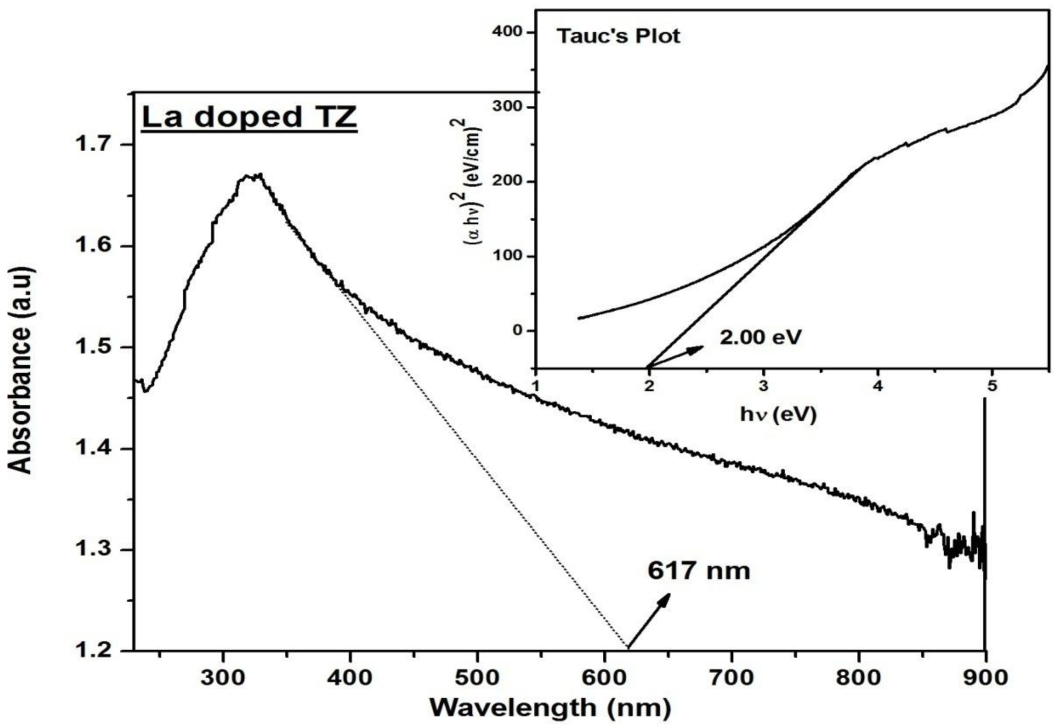

Figure 21: Absorption spectrum and Tauc's plot for La doped TiO_2-ZrO_2 composite

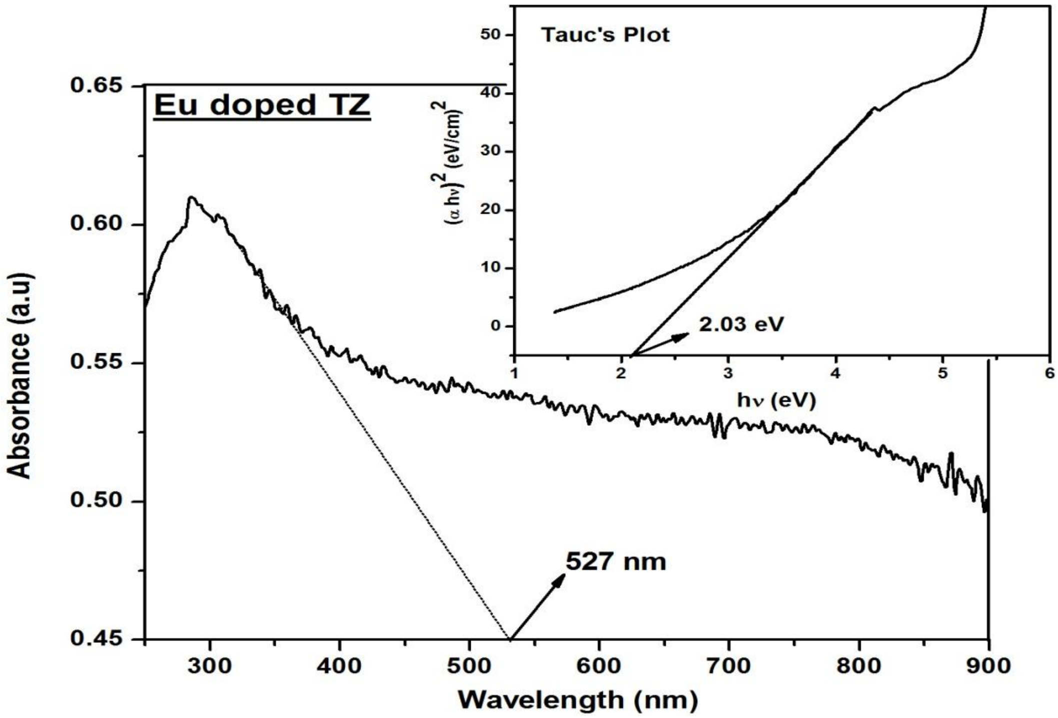

Figure 22: Absorption spectrum and Tauc's plot for Eu doped TiO_2-ZrO_2 composite

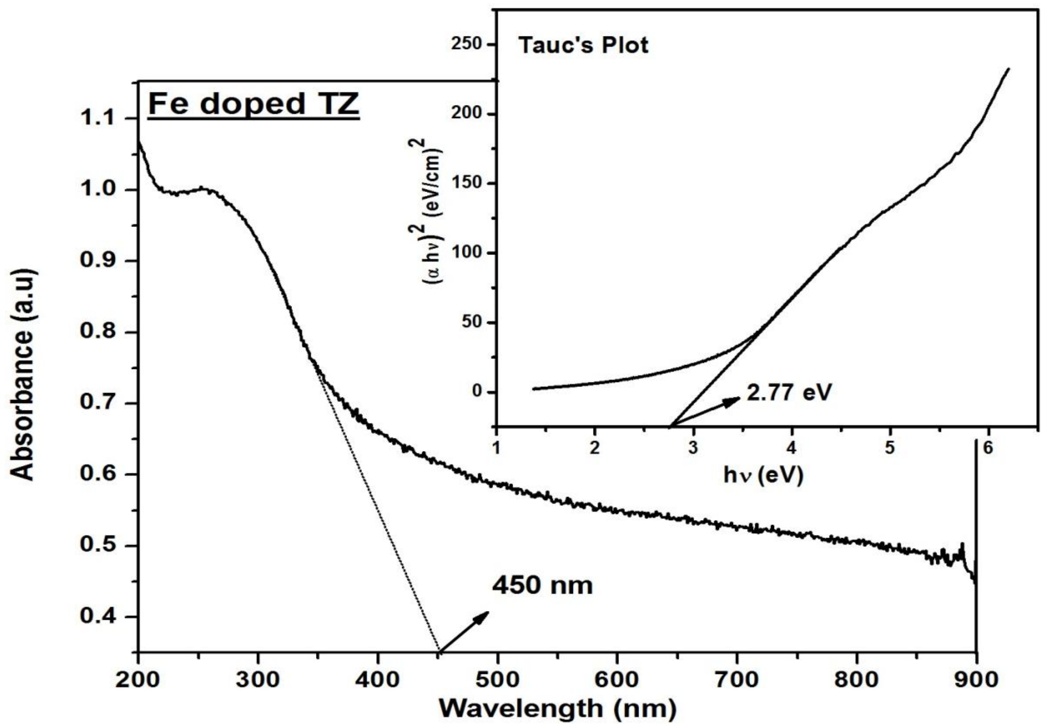

Figure 23: Absorption spectrum and Tauc's plot for Fe doped TiO_2-ZrO_2 composite

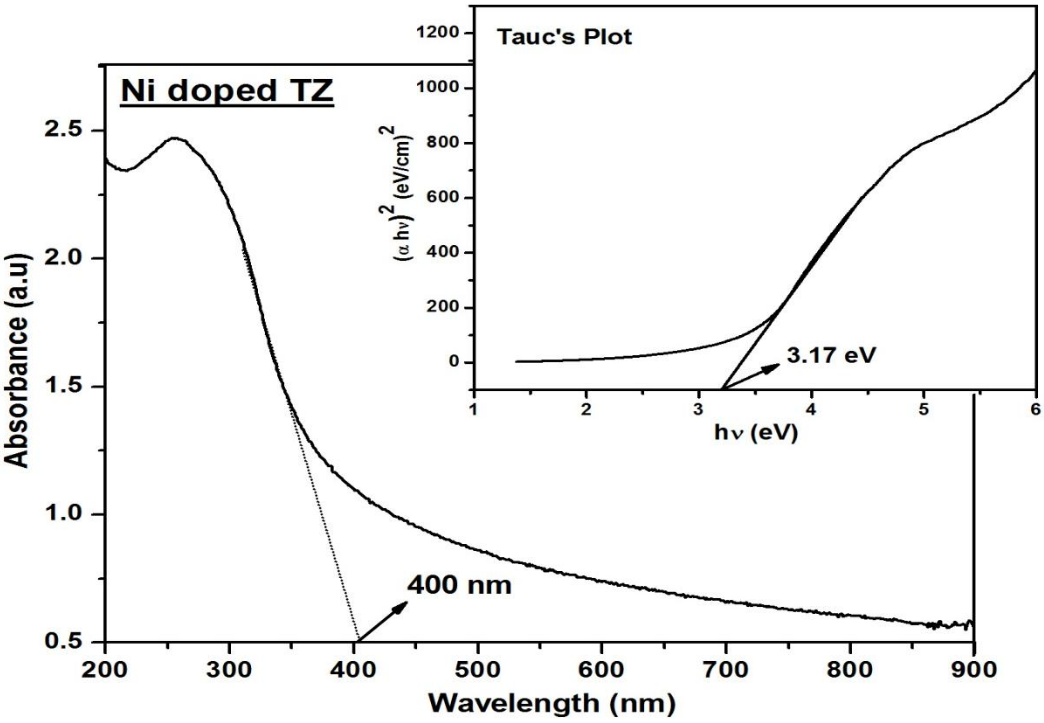

Figure 24: Absorption spectrum and Tauc's plot for Ni doped TiO_2-ZrO_2 composite

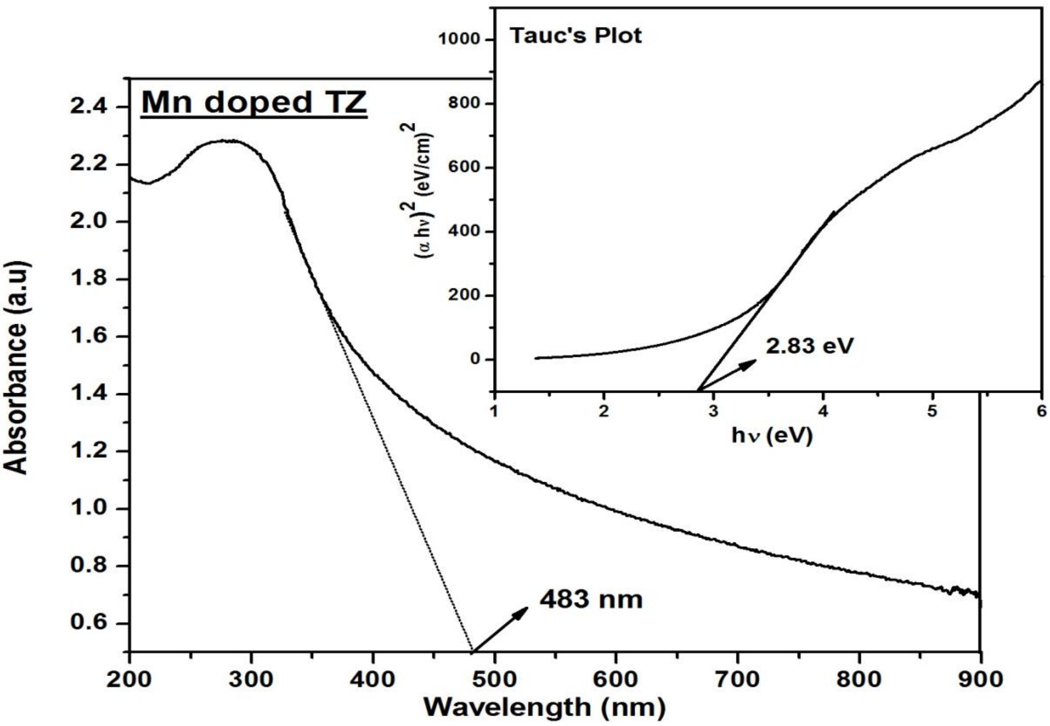

Figure 25: Absorption spectrum and Tauc's plot for Mn doped TiO_2-ZrO_2 composite

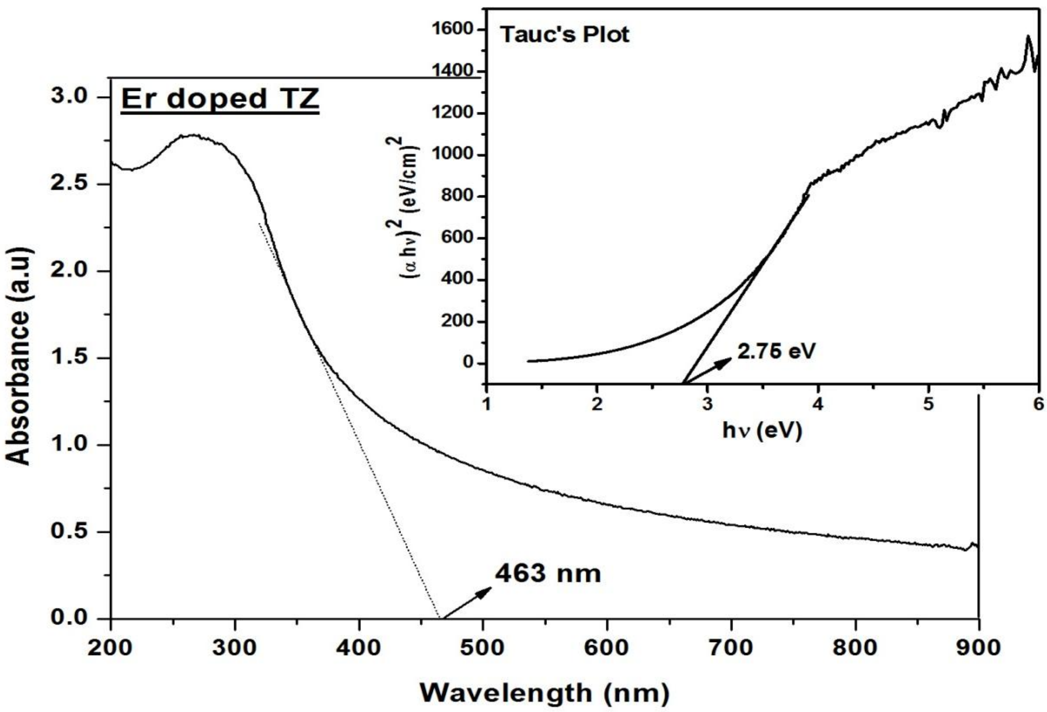

Figure 26: Absorption spectrum and Tauc's plot for Er doped TiO_2-ZrO_2 composite

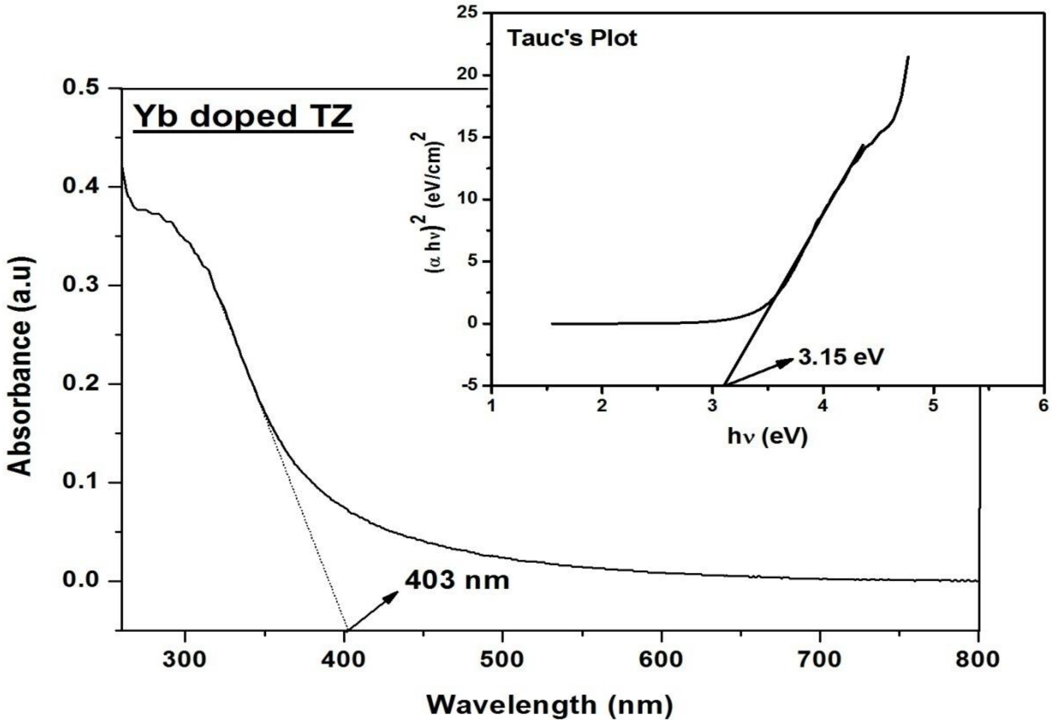

Figure 27: Absorption spectrum and Tauc's plot for Yb doped TiO_2-ZrO_2 composite

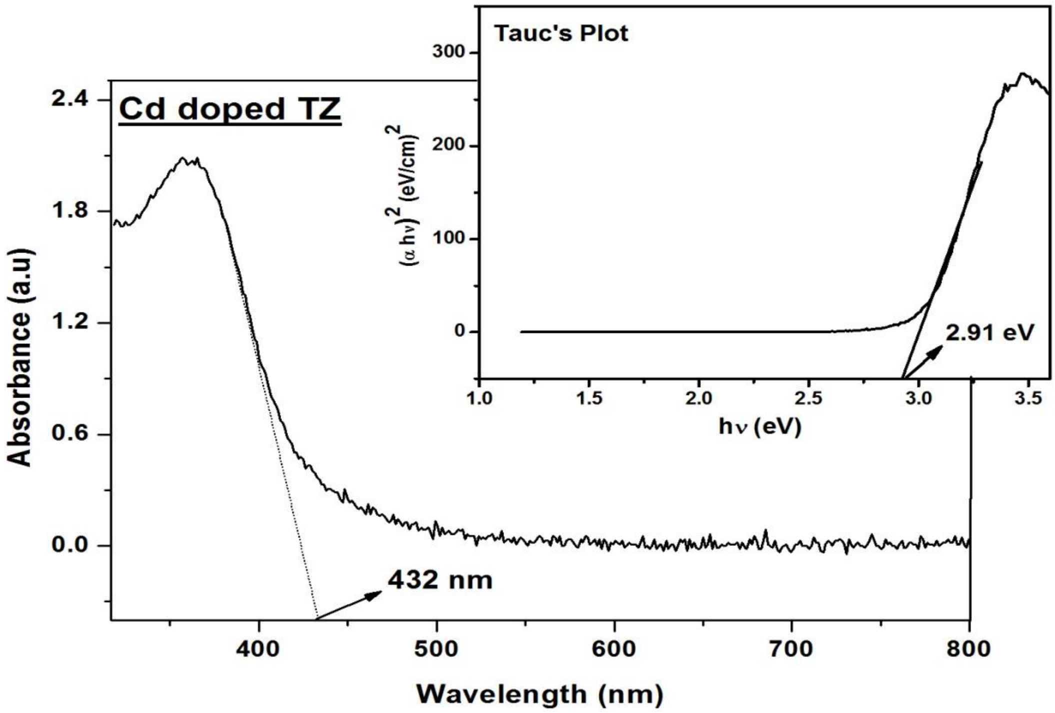

Figure 28: Absorption spectrum and Tauc's plot for Cd doped TiO_2-ZrO_2 composite

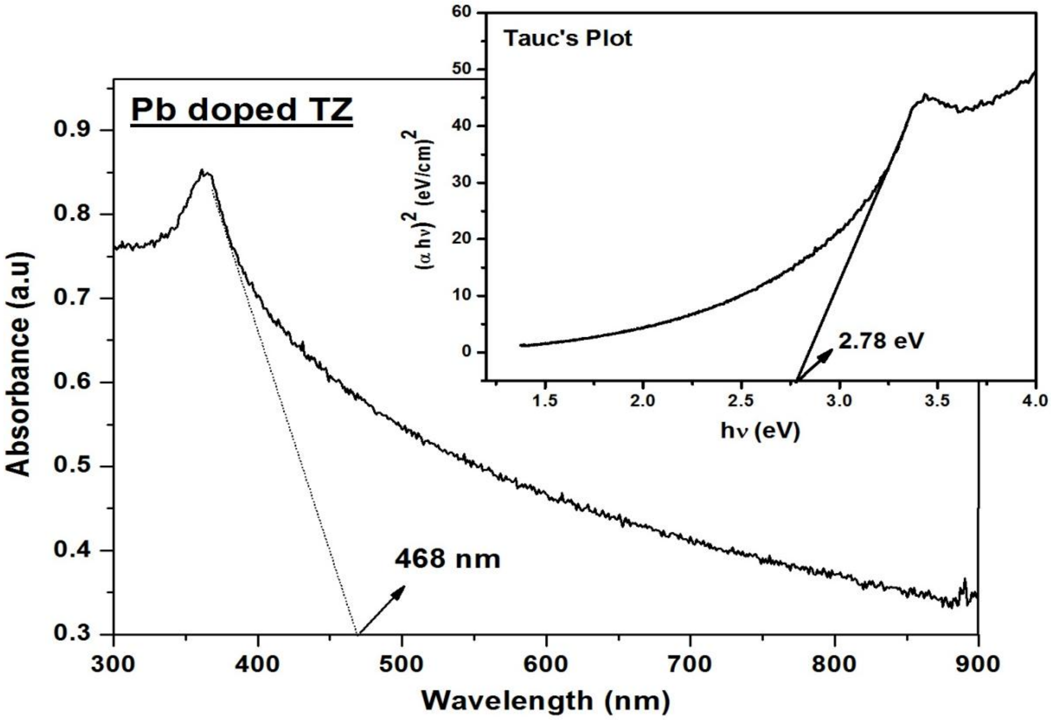

Figure 29: Absorption spectrum and Tauc's plot for Pb doped TiO_2-ZrO_2 composite

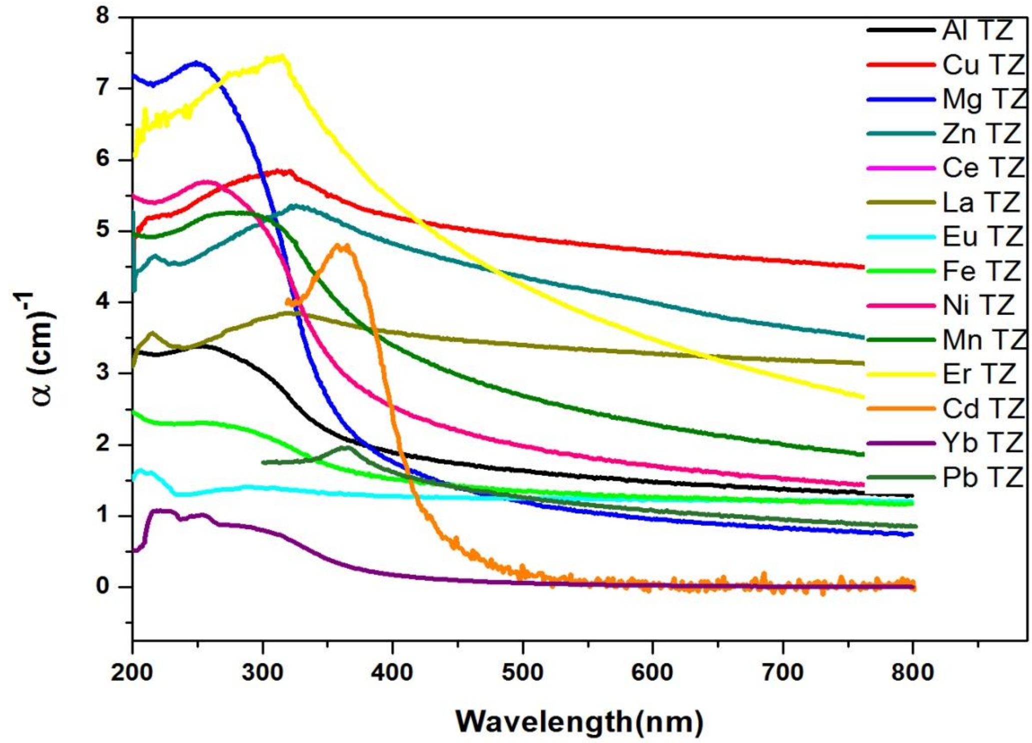

Figure 30: Variation of absorption coefficient with wavelength

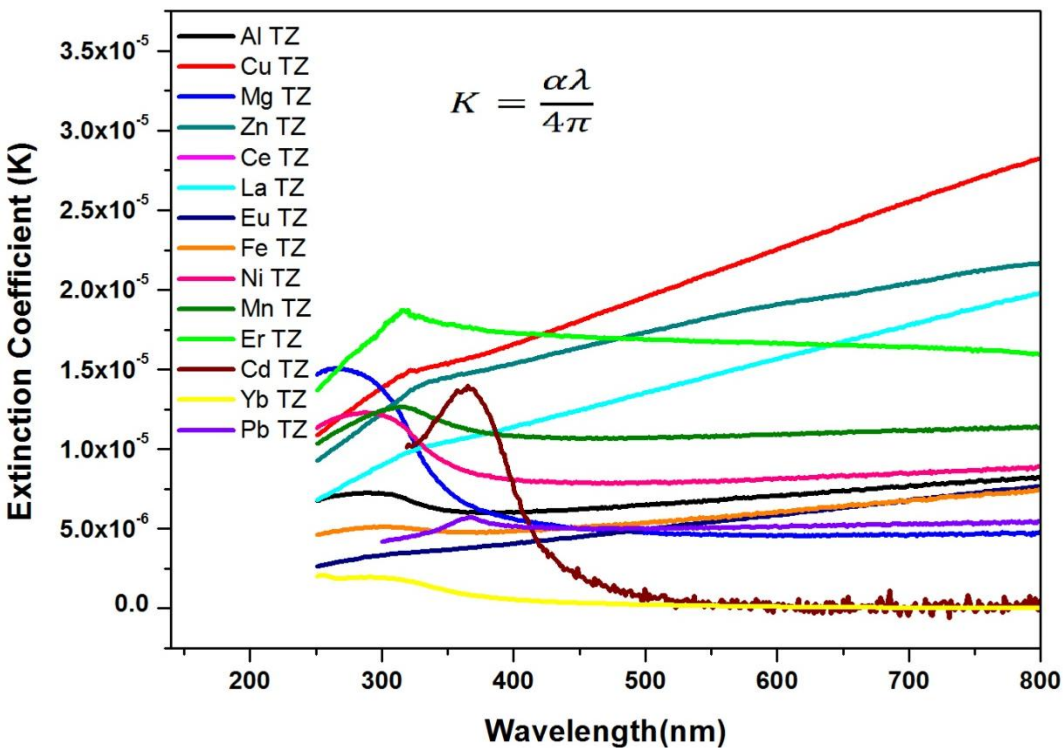

Figure 31: Variation of extinction coefficient with wavelength

Table 16: Optical parameters of metal doped TiO_2-ZrO_2

Sample	Peak Absorption (nm)	Optical Bandgap	Refractive Index
Al doped TZ	253	2.96 eV	2.37
Cu doped TZ	320	2.40 eV	2.54
Mg doped TZ	249	3.34 eV	2.28
Zn doped TZ	325	2.04 eV	2.67
Ce doped TZ	314	2.68 eV	2.45
La doped TZ	327	2.00 eV	2.69
Eu doped TZ	285	2.03 eV	2.68
Fe doped TZ	256	2.77 eV	2.42
Ni doped TZ	256	3.17 eV	2.32
Mn doped TZ	285	2.83 eV	2.41
Er doped TZ	265	2.75 eV	2.43
Yb doped TZ	275	3.15 eV	2.32
Cd doped TZ	360	2.91 eV	2.38
Pb doped TZ	363	2.78 eV	2.42

6.4 Conclusion

By looking at the structural parameters it can be concluded that metal doping have lowered the crystallite size and stabilized the Anatase phase of TiO_2. Sample doped with La, Cd, Yb, and Pb contains TiO_2 purely in Anatase phase. Optical properties revealed that metal doping has increased the absorption in visible region.

References

[1] Anh Tuan Vu, Quoc Tuan Nguyen, Thi Hai Linh Bui, Manh Cuong Tran, Tuyet Phuong Dang and Thi Kim Hoa Tran, Adv. Nat. Sci, Nanosci. Nanotechnol, 2010, , 015009.

[2] Long Wang, Jian Mao, Gao-Hua Zhang, Ming-Jing Tu, World J Gastroenterol, 2007, 13, 4011-4014.

[3] Jianhua Chen, Maosheng Yao, Xiaolin Wang, J Nanopart Res, 2008, 10, 163–171.

[4] W. Choi, A. Termin, M.R. Hoffmann, J. Phys. Chem, 994, 98, 13669.

[5] A. Kaushik, B. Dalela, Sudhish Kumar, P.A. Alvi, S. Dalela, Journal of Alloys and Compounds, 2013, 552, 274.

[6] Aytac Gultekin, Material Science, 2014, 20, 1.

[7] S. T. Hussain, A. Siddiqa, Int. J. Environ. Sci. Tech., 2011, 8, 351

[8] Dr.Selma, M.Hassan, Al-Jawad, International Journal of Scientific & Engineering Research, 2014, 5.

[9] D.H. Kim, S.I.Woo, S.H. Moon, H.D. Kim, B.Y. Kim, J.H. Cho, Y.G. Joh, E.C. Kim, Effect of Co/Fe co-doping in TiO2 rutile prepared by solid state reaction, Solid State Commun. 136 (2005) 554.

[10] L. Jing, X. Sun, B. Xin, B. Wang, W. Cai, H. Fu, J. Solid State Chem, 2004, 177, 3375.

[11] Y. Zhang, H. Xu, Y. Xu, H. Zhang, Y. Wang, J. Photochem. Photobiol. Chem, 2005, 170, 279.

[12] X. Yan, J. He, D.G. Evans, X. Duan, Y. Zhu, Appl. Catal. B: Environ, 2005, 55, 243.

[13] Y. Xie, C. Yuan, X. Li, Mater. Sci. Eng. B, 2005, 117, 325.

[14] J. Tian, H. Gao, H. Kong, P. Yang, W. Zhang and J. Chu, Nanoscalre Research Lett. 2013, 8.

[15] Jina Choi, Hyunwoong Park and Michael R. Hoffmann, J. Phys. Chem, 2010, 114, 783–792.

[16] A. Mendoza-Galvan and C. Trejo-Cruz, 2006, 99.

[17] Yang Wang, Wubiao Duan, Bo Liu, Xidong Chen, Feihua Yang and Jianping Guo, Journal of Nanomaterials, 2014, 2014, 1

[18] M. Effendi and Bilalodin, International Journal of Basic and Applied Science, 2012, 12, 107.

[19] G. Magesh, B. Vishwanathan, R. P. Vishwanath, T. K. Varadarajan, Indian Journal of Chemistry, 2009, 48, 480-488.

[20] A. K. Zak, W. H. Abd. Majid, M. E. Abrishami and R. Yousefi R, Solid State Sciences, 2011, 13, 251–256.